Europe PMC Funders Group
Author Manuscript
Nature. Author manuscript; available in PMC 2019 February 15.

Published in final edited form as:
Nature. 2018 August ; 560(7719): 453–455. doi:10.1038/s41586-018-0401-y.

Atomic iron and titanium in the atmosphere of the exoplanet KELT-9b

H. Jens Hoeijmakers[1,2], **David Ehrenreich**[1], **Kevin Heng**[2,*], **Daniel Kitzmann**[2], **Simon L. Grimm**[2], **Romain Allart**[1], **Russell Deitrick**[2], **Aurélien Wyttenbach**[1], **Maria Oreshenko**[2], **Lorenzo Pino**[1], **Paul B. Rimmer**[3,4], **Emilio Molinari**[5,6], and **Luca Di Fabrizio**[5]

[1]Observatoire astronomique de l'Université de Genève, Versoix, Switzerland [2]University of Bern, Center for Space and Habitability, Bern, Switzerland [3]University of Cambridge, Cavendish Astrophysics, Cambridge, UK [4]MRC Laboratory of Molecular Biology, Cambridge, UK [5]INAF FGG, Telescopio Nazionale Galileo, Breña Baja, Spain [6]INAF Osservatorio Astronomici di Cagliari, Selargius, Italy

Abstract

To constrain the formation history of an exoplanet, we need to know its chemical composition1–3. With an equilibrium temperature of about 4,050 kelvin4, the exoplanet KELT-9b (also known as HD 195689b) is an archetype of the class of ultrahot Jupiters that straddle the transition between stars and gas-giant exoplanets and are therefore useful for studying atmospheric chemistry. At these high temperatures, iron and several other transition metals are not sequestered in molecules or cloud particles and exist solely in their atomic forms5. However, despite being the most abundant transition metal in nature, iron has not hitherto been detected directly in an exoplanet because it is highly refractory. The high temperatures of KELT-9b imply that its atmosphere is a tightly constrained chemical system that is expected to be nearly in chemical equilibrium5 and cloud-free6,7, and it has been predicted that spectral lines of iron should be detectable in the visible range of wavelengths5. Here we report observations of neutral and singly ionized atomic iron (Fe and Fe) and singly ionized atomic titanium (Ti) in the atmosphere of KELT-9b. We identify these species using cross-correlation analysis8 of high-resolution spectra obtained as the exoplanet passed in front of its host star. Similar detections of metals in other ultrahot Jupiters will provide constraints for planetary formation theories.

Motivated by theoretical predictions5, we conducted a search for metal lines in the high-resolution transmission spectrum of KELT-9b, which was observed using the HARPS-North (HARPS-N) spectrograph during a single transit of the exoplanet. HARPS-N is a fibre-fed spectrograph, stabilized in pressure and temperature and mounted on the 3.58-m Telescopio

* kevin.heng@csh.unibe.ch.

Data availability. The observations that support the findings of this study were obtained as part of DDT programme A35DDT4 and are available in the public archive of the TNG (http://ia2.oats.inaf.it/archives/tng).

Code availability. All codes, programs and algorithms that were used to support the findings of this study are described in previously published literature. The codes to calculate the opacity functions and to model atmospheric chemistry are publicly available at https://github.com/exoclime.

Europe PMC Funders Author Manuscripts
Europe PMC Funders Author Manuscripts

Europe PMC Funders Author Manuscripts

Europe PMC Funders Author Manuscripts

Nazionale Galileo (TNG), which is located on the Canary Island of La Palma, Spain. We recorded 19 and 30 spectra during the 3.9-h-long transit and outside of this transit, respectively, covering the whole night from 31 July 2017 to 1 August 2017. Spectra were reduced with the HARPS-N data reduction software, version 3.8. They consist of 69 orders covering the wavelength range 3,874–6,909 Å and overlapping partially at their edges. Orders were extracted individually, flat-fielded using calibrations obtained during twilight, and deblazed and wavelength-calibrated in the Solar System barycentric rest frame. We built a common reference-wave- length grid with a spectral resolution of 0.01 Å, on which the calibrated orders were then binned. Pixels in overlapping orders at the same wave- length were then averaged to conserve the flux. Contamination of the spectra by absorption lines of Earth's atmosphere (mainly by water) were corrected using established methods (see Methods). The optical range of wavelengths is populated with electronic transitions of atoms and ions of metals. With a spectral resolving power of about 115,000, these data are ideal for searching for the absorption signatures associated with metals present in the atmosphere of KELT-9b, by cross-correlating the high-resolution spectra8,9 with theoretical templates constructed from the cross-sections of the relevant species10 (Fig. 1).

We searched specifically for the spectral lines of Fe, Fe , neutral titanium (Ti) and Ti in the data because the relative abundances of these species vary by many orders of magnitude between atmospheric temperatures of 2,500 K and 6,000 K (Fig. 1). Fe becomes more abundant than Fe at about 3,900–4,300 K, depending on whether chemical equilibrium is assumed (Fig. 1c) or whether photochemistry and vertical mixing are present (Fig. 1d); Ti becomes more abundant than Ti at about 3,000–3,400 K. These estimates assume that the elemental abundances (C/H, O/H, N/H, Ti/H and Fe/H) are equal to those of the Sun; that is, they assume solar metallicity. The abundances of Fe and Ti stabilize above the transition temperatures quoted above (Fig. 1), meaning that only lower bounds on the atmospheric temperature of KELT-9b may be obtained.

Observing through the atmosphere of Earth means that the measured transmission spectrum lacks an absolute empirical normalization. This lack of an absolute empirical normalization implies that absolute atomic abundances cannot be extracted from the data, which in turn implies that the metallicity cannot be inferred from these data alone. In addition, model transmission spectra lack an absolute theoretical normalization11–13. In most hot Jupiters, the spectral continuum is dominated by a combination of Rayleigh scattering associated with molecular hydrogen, the spectral line wings of molecules and the alkali metals (which are mediated by pressure broadening), collision-induced absorption associated with helium and molecular hydrogen, and clouds or hazes. For KELT-9b, the unusually high temperatures imply that all species are in the gas phase and that opacity as a result of bound-free absorption associated with hydrogen anions (H^-)14 is the dominant source of the spectral continuum15 rather than Rayleigh scattering associated with atomic and molecular hydrogen (Fig. 1). The line wings of Fe, Fe , Ti and Ti are also subdominant (Fig. 1), which implies that pressure-broadening is not a source of uncertainty.

This rather peculiar property of KELT-9b, and of ultrahot Jupiters in general, allows us to meaningfully compute the relative differences between the line peaks of Fe, Fe , Ti and Ti and the spectral continuum provided by H^-. We construct four templates, using theoretical

Europe PMC Funders Author Manuscripts

Europe PMC Funders Author Manuscripts

transmission spectra13 that consist separately of Fe, Fe , Ti and Ti lines, each with a H^- continuum. The ability to determine the relative normalization between the line peaks and the continuum means that we are able to give more weight to strong lines and less weight to weak lines in our templates, which results in a higher signal-to-noise ratio in our cross-correlations compared to an analysis using templates in which all of the lines are weighted equally (a so-called binary mask).

Encoded in the data are two distinct signatures: the rotation of the star ($v\sin i$ = 111.4 km s −1, where v is the rotational velocity and i is the projected angle of the spin axis) and the orbital velocity of the exoplanet (±81 km s^{-1}), both projected along the line of sight to the observer. Each location on the stellar disk corresponds to a different projected rotational velocity of the star. As the exoplanet moves across the stellar disk, it traces out a range of projected rotational velocities with time (Fig. 2). This leaves an imprint on each stellar absorption line that shows up as an enhancement in flux at the wavelength that corresponds to the projected rotational velocity. When the time-averaged stellar spectrum is subtracted from the data and the cross-correlation analysis is performed, a time-dependent residual known as a Doppler shadow remains (Fig. 2). The tilt of the Doppler shadow with respect to the axes of time and wavelength can be used to infer the angle between the rotational axis of the star and the orbital plane of the exoplanet. This Doppler tomo-graphy technique was used previously to infer that KELT-9b resides in a near-polar orbit4. Superimposed on the Doppler shadow is the time- dependent absorption spectrum of the atmosphere of KELT-9b (Fig. 2). The spectrum shifts in wavelength with time because it is associated with the varying projected orbital velocity of the exoplanet.

To perform the cross-correlations, we subdivided the reduced spectra into 20-nm bins (for computational efficiency), each to be treated independently in the analysis. We measured the stellar spectrum by averaging the out-of-transit exposures, divided the master stellar spectrum that we obtained out of each exposure and corrected for residual fluctuations in the continuum by normalizing each spectrum using a smoothing filter (with a width of 0.75 Å). Each spectral pixel is weighted by the reciprocal of its variance in time8. The Doppler shadow is subtracted to isolate the atmospheric signal from the exoplanet (see Methods). We cross-correlated the residuals between radial velocities of 1,000 km s^{-1} with the templates.

The peaks in the cross-correlation function (CCF) of Fe, Fe and Ti are seen as bright streaks across the axes of time and systemic radial velocity (Fig. 3). These streaks were also seen in the discovery study4 and are presumably caused by spectral lines that the exoplanet and the star have in common, notably Fe . Co-adding the signal along these streaks, in the rest frame of the exoplanet, results in significant detections of CCF peaks for Fe, Fe and Ti with signal-to-noise ratios of 7, 14 and 9, respectively. The CCFs are normalized by the standard deviation at velocities away from the rest frame of the exoplanet to produce the signal-to-noise ratios of the detections. By fitting Gaussians to these CCFs, we find weighted average line contrasts of (0.28 0.03) 10^{-3} (9.3), (2.21 0.08) 10^{-3} (26) and (1.28 0.07) 10^{-3} (18) for Fe, Fe and Ti , respectively. The Gaussian standard deviation is denoted by and the uncertainties quoted are 1 . There is no significant detection of the CCF for Ti, which has an average line contrast of (0.18 0.05) 10^{-3} (3.3).

Europe PMC Funders Author Manuscripts

Europe PMC Funders Author Manuscripts

That the lines of Fe show up more prominently than those of Fe suggests that the atmospheric temperatures probed exceed about 4,000 K. The non-detection of Ti (Fig. 3) supports this interpretation. The discovery of Fe, Fe and Ti in KELT-9b sets the stage for future searches for carbon monoxide (CO) and water (H_2O) in the near-infrared range of wavelengths. At these elevated temperatures, CO is expected to be the dominant molecule, which would imply that its abundance directly mirrors the value of C/H (for C/O 1) or O/H (for C/O 1)5. Detecting H_2O would enable the carbon-poor and carbon-rich scenarios to be distinguished16,17. Inferring C/H and O/H would allow the metallicity to be constrained. These prospects ensure that KELT-9b will remain important for studying extrasolar atmospheric chemistry using both space- and ground-based telescopes.

Methods

Telluric lines are the main contaminant in the observed spectrum, with strong spectral lines of water and molecular oxygen in the visible range of wavelengths. To perform decontamination, we used version 1.5.1 of Molecfit18, an ESO tool for correcting for the tellurics in ground-based spectra following established procedures19. We tested the performance of our telluric correction by cross-correlating the corrected and uncorrected in-transit spectra with a telluric water-absorption template spectrum (at 296 K). Extended Data Fig. 1 demonstrates that our correction efficiently removes the telluric water signal.

To remove the Doppler shadow, we cross-correlated the data with a PHOENIX stellar model template that matches the effective temperature of the star20. We modelled and fitted the main Doppler shadow that occurs near −35 km s^{-1}, as well as three aliases near 80 km s^{-1}, 20 km s^{-1} and −125 km s^{-1}, as time- dependent Gaussians. The best-fit parameters (central radial velocity, width and amplitude) are described by first-, second-, third- or fourth-degree polynomials in time. The resulting model of the Doppler shadow was adjusted in amplitude to the CCF obtained for each species and subtracted. We applied a cross-correlation formalism as used previously19 to measure the average line strengths of Fe, Fe , Ti and Ti . For this purpose, the templates that were used to detect the species were continuum-subtracted to act as weighted binary masks that measure the aver- age spectral line present in each spectral bin and each exposure. The final one- dimensional CCFs were obtained by a weighted co-addition of the 20 bins and 19 in-transit exposures following the same strategy as used previously21. The weights were obtained by injecting the templates into the data at the start of the analysis at a low level as to not affect the statistics of the CCF22, and subsequently measuring the resulting increase in the CCF. Wavelength regions with poorer data quality or fewer spectral lines of the target species were thereby implicitly given a low weight.

The opacities10 of Fe, Fe , Ti and Ti were computed using standard methods23,24 and the open-source HELIOS-K opacity calculator25. Equilibrium-chemistry calculations were performed using the FastChem code26. We note that the JANAF database (https://janaf.nist.gov) supplies the Gibbs free energies needed to perform the equilibrium-chemistry calculations up to only 6,000 K. Chemical-kinetics calculations were performed using the ARGO code27. The templates for the neutrals (Fe, Ti) and ions (Fe , Ti) assume atmospheric temperatures of 3,500 K and 4,500 K, respectively; assuming different

Europe PMC Funders Author Manuscripts

Europe PMC Funders Author Manuscripts

temperatures results in slight changes to the signal-to-noise ratio of each detection. The bright CCF streaks associated with each species were co-added along each streak, in the rest frame of the exo-planet, by using the measured orbital parameters4 and experimenting with a range of values for the orbital velocity of the exoplanet. We estimate the signal-to-noise ratios of the individually detected species by measuring the standard deviation of the CCF at velocities more than 50 km s^{-1} away from the exoplanet's rest frame. Water was not detected below the 200 p.p.m. level (3).

Extended Data

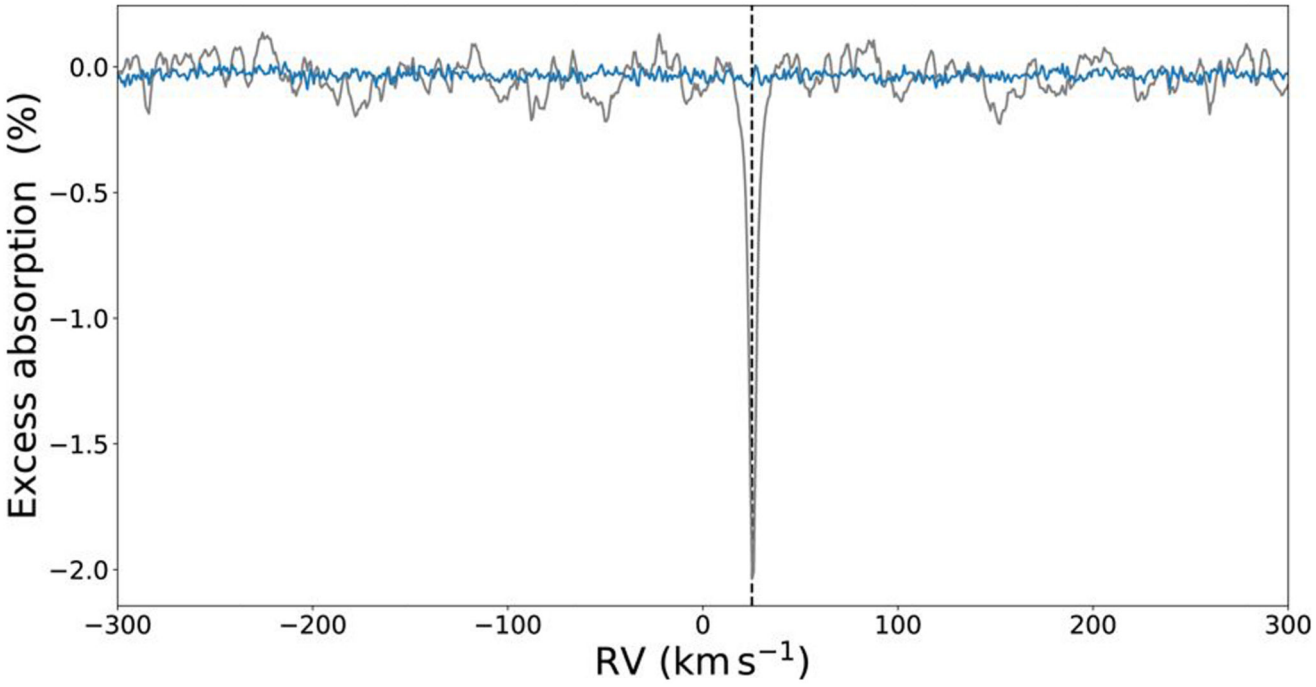

Extended Data Fig. 1.

Telluric water-absorption correction. Crosscorrelation analysis performed on the in-transit spectrum with a telluric water-absorption template spectrum (at 296 K). The blue and grey curves are the transit depths with and without the telluric correction, respectively. The data are shifted to the rest frame of the star, such that the signal dominated by telluric water absorption occurs near +25 km s^{-1} (corresponding to the barycentric Earth radial velocity (BERV) systemic velocity), as indicated by the dashed vertical line.

Supplementary Material

Refer to Web version on PubMed Central for supplementary material.

References

1. Öberg KI, Murray-Clay R, Bergin EA. The effects of snowlines on C/O in planetary atmospheres. Astrophys J. 2011; 743:L16.

Europe PMC Funders Author Manuscripts

2. Madhusudhan N, Amin MA, Kennedy GM. Toward chemical constraints on hot jupiter migration. Astrophys J. 2014; 794:L12.
3. Öberg KI, Bergin EA. Excess C/O and C/H in outer protoplanetary disk gas. Astrophys J. 2016; 831:L19.
4. Gaudi BS, et al. A giant planet undergoing extreme-ultraviolet irradiation by its hot massive-star host. Nature. 2017; 546:514–518. [PubMed: 28582774]
5. Kitzmann D, et al. The peculiar atmospheric chemistry of KELT-9b. Astrophys J. 2018
6. Heng K. A cloudiness index for transiting exoplanets based on the sodium and potassium lines: tentative evidence for hotter atmospheres being less cloudy at visible wavelengths. Astrophys J. 2016; 826:L16.
7. Stevenson KB. Quantifying and predicting the presence of clouds in exoplanet atmospheres. Astrophys J. 2016; 817:L16.
8. Snellen IAG, de Kok RJ, de Mooij EJW, Albrecht S. The orbital motion, absolute mass and high-altitude winds of exoplanet HD209458b. Nature. 2010; 465:1049–1051. [PubMed: 20577209]
9. Brogi M, et al. The signature of orbital motion from the dayside of the planet τ Boötis b. Nature. 2012; 486:502–504. [PubMed: 22739313]
10. Kurucz RL. Including all the lines: data releases for spectra and opacities. Can J Phys. 2017; 95:825–827.
11. Benneke B, Seager S. Atmospheric retrieval for super-Earths: uniquely constraining the atmospheric composition with transmission spectroscopy. Astrophys J. 2012; 753:100.
12. Griffith CA. Disentangling degenerate solutions from primary transit and secondary eclipse spectroscopy of exoplanets. Philos Trans R Soc Lond A. 2014; 372
13. Heng K, Kitzmann D. The theory of transmission spectra revisited: a semi-analytical method for interpreting WFC3 data and an unresolved challenge. Mon Not R Astron Soc. 2017; 470:2972–2981.
14. John TL. Continuous absorption by the negative hydrogen ion reconsidered. Astron Astrophys. 1988; 193:189–192.
15. Arcangeli J, et al. H− opacity and water dissociation in the dayside atmosphere of the very hot gas giant WASP-18b. Astrophys J. 2018; 855:L30.
16. Madhusudhan N. C/O ratio as a dimension for characterizing exoplanetary atmospheres. Astrophys J. 2012; 758:36.
17. Heng K, Tsai S-M. Analytical models of exoplanetary atmospheres. III. Gaseous C–H–O–N chemistry with nine molecules. Astrophys J. 2016; 829:104.
18. Smette A, et al. Molecfit: a general tool for telluric absorption correction. I. Method and application to ESO instruments. Astron Astrophys. 2015; 576:A77.
19. Allart R, et al. Search for water vapor in the high-resolution transmission spectrum of HD 189733b in the visible. Astron Astrophys. 2017; 606:A144.
20. Husser T-O, et al. A new extensive library of PHOENIX stellar atmospheres and synthetic spectra. Astron Astrophys. 2013; 553:A6.
21. Hoeijmakers HJ, et al. A search for TiO in the optical high-resolution transmission spectrum of HD 209458b: hindrance due to inaccuracies in the line database. Astron Astrophys. 2015; 575:A20.
22. Brogi M, et al. Rotation and winds of exoplanet HD 189733 b measured with high-dispersion transmission spectroscopy. Astrophys J. 2016; 817:106.
23. Rothman LS, et al. The HITRAN molecular spectroscopic database and HAWKS (HITRAN atmospheric workstation): 1996 edition. J Quant Spectrosc Rad Trans. 1998; 60:665–710.
24. Heng, K. Exoplanetary Atmospheres: Theoretical Concepts and Foundations. Princeton Univ. Press; Princeton: 2017. 74–81.
25. Grimm SL, Heng K. HELIOS-K: an ultrafast, open-source opacity calculator for radiative transfer. Astrophys J. 2015; 808:182.
26. Stock JW, Kitzmann D, Patzer ABC, Sedlmayr E. FastChem: a computer program for efficient complex chemical equilibrium calculations in the neutral/ ionized gas phase with applications to stellar and planetary atmospheres. Mon Not R Astron Soc. 2018; 479:865–874.

27. Rimmer PB, Helling Ch. A chemical kinetics network for lightning and life in planetary atmospheres. Astrophys J Suppl Ser. 2016; 224:9.

Europe PMC Funders Author Manuscripts

Europe PMC Funders Author Manuscripts

Europe PMC Funders Author Manuscripts

Europe PMC Funders Author Manuscripts

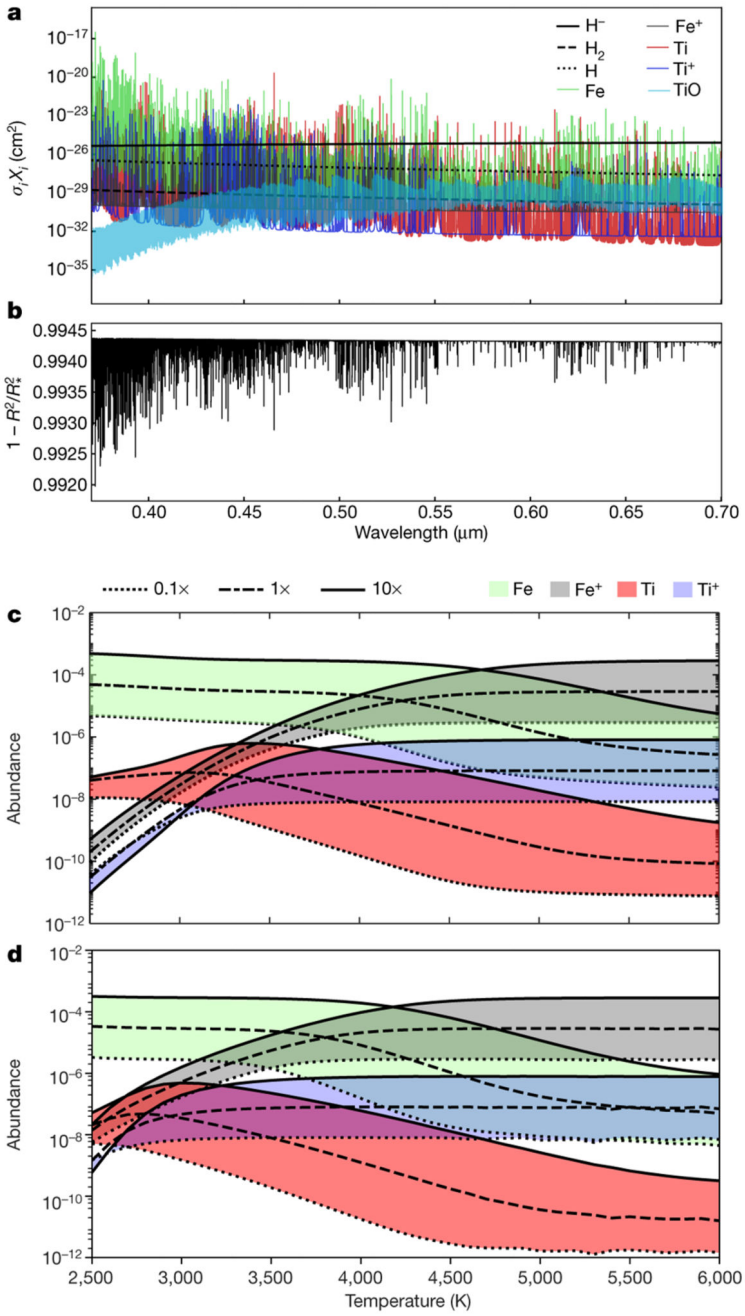

Fig. 1. Theoretical cross-sections and chemistry.

a, Cross-sections σ_i of Rayleigh scattering associated with atomic and molecular hydrogen (H and H_2), bound-free absorption associated with the hydrogen anion (H^-) and the spectral lines of neutral and singly ionized iron and titanium (Fe, Fe^+, Ti and Ti^+) and of titanium oxide (TiO), weighted by their relative abundances by number (volume mixing ratios X_i), assuming chemical equilibrium, a temperature of 4,000 K and solar metallicity. The dominance of H^- absorption implies that the spectral continuum can be used to estimate the pressure associated with the transit chord probed in KELT-9b, which we compute to be

about 10 mbar. b, The theoretical transmission spectrum corresponding to the cross-sections shown. R and R_* denote the exoplanetary and stellar radii, respectively. c, Mixing ratios of Fe, Fe^+, Ti and Ti^+ as a function of temperature, assuming chemical equilibrium and for metallicities of 0.1, 1 and 10 times the solar metallicity. d, Same as c, but including photochemistry and a representative vertical mixing strength of 1010 $cm^2\ s^{-1}$.

Europe PMC Funders Author Manuscripts

Europe PMC Funders Author Manuscripts

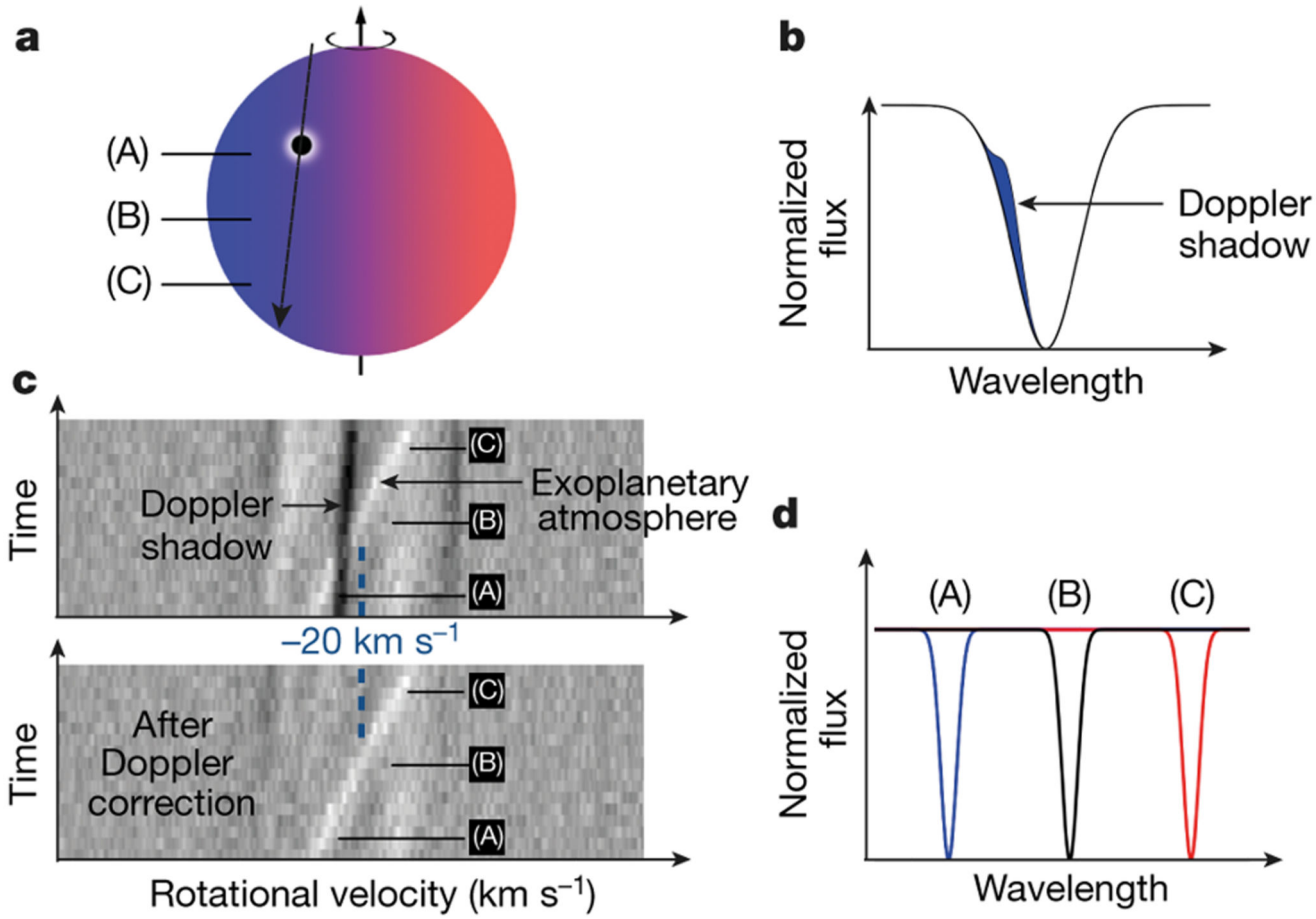

Fig. 2. Geometry of the KELT-9 system.

a, Schematic of the orbital geometry of the exoplanet (represented by the black filled circle). The arrow indicates the orbital trajectory of the exoplanet as it transits across the stellar disk. The blue and red shading represent the blue- and redshifted regions on the stellar disk caused by stellar rotation. b, The obscuration of part of the stellar disk results in an enhancement in flux of the stellar absorption line, as indicated by the blue shaded area. d, Furthermore, as the exoplanet progresses in its orbit, its projected orbital velocity shifts from being blueshifted (at point A) to being redshifted (at point C). c, These two distinct signatures show up in the cross-correlation function (CCF; grey scale; top) as a Doppler shadow (deficit in the CCF at the instantaneous velocity of the obscured part of the stellar disk) and a bright streak (enhancement in the CCF at the instantaneous radial component of the orbital velocity of the planet), respectively. To isolate the signature of the planet, we model and subtract the Doppler shadow from the CCF (bottom). The systemic radial velocity of the KELT-9 system (−20 km s^{-1}) is indicated.

Europe PMC Funders Author Manuscripts
Europe PMC Funders Author Manuscripts

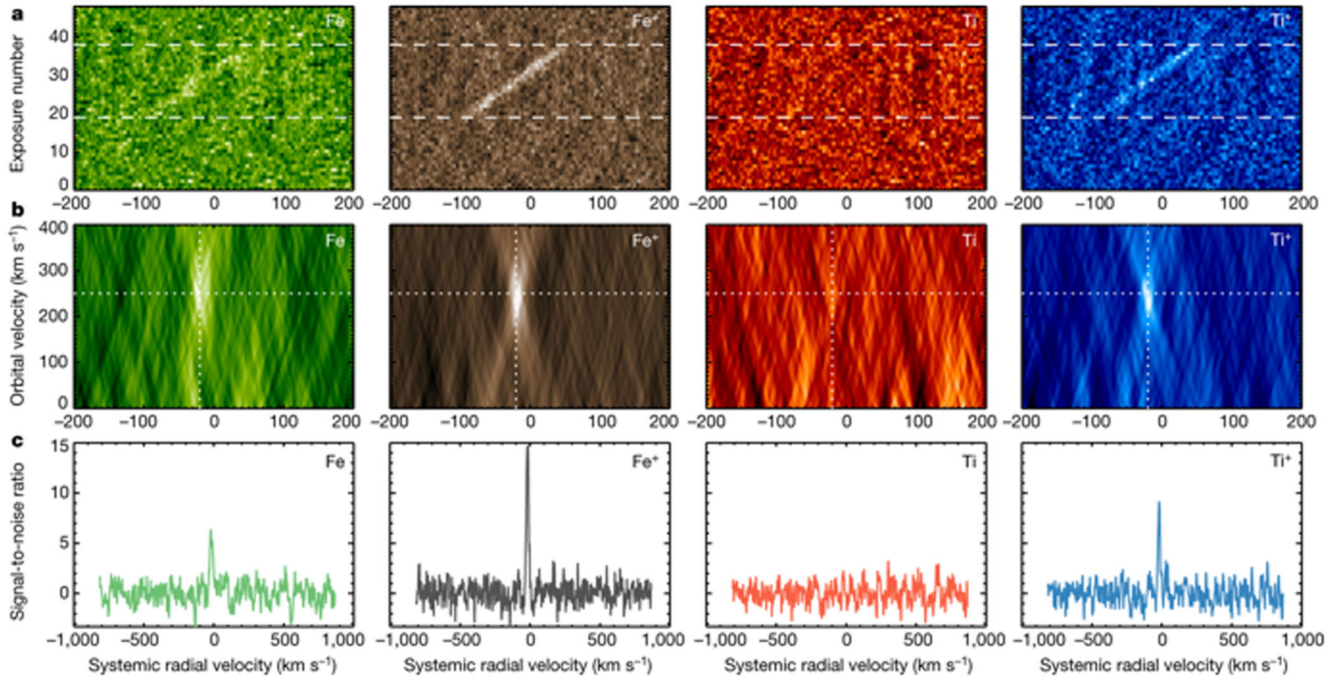

Fig. 3. Analysis of observations.

Separate cross-correlation analyses were performed using templates with Fe, Fe^+, Ti and Ti^+. Each template assumes a spectral continuum associated with H^-. a, CCFs (colour scale) with the Doppler shadow subtracted. The absorption spectrum of the exoplanetary atmosphere shows up as a bright streak. The horizontal dashed lines mark the start and end of transit. b, The CCFs co-added along each streak (that is, in the rest frame of the exoplanet). The horizontal and vertical dotted lines denote the expected orbital velocity of KELT-9b and the systemic velocity of the KELT-9 system, respectively. c, The signal-to-noise ratio of cross-correlation extracted at an orbital velocity of 254 km s^{-1}. Fe, Fe^+ and Ti^+ are clearly detected, but Ti is not.

Europe PMC Funders Author Manuscripts
Europe PMC Funders Author Manuscripts